Data in Brief 41 (2022) 107863

Contents lists available at ScienceDirect

Data in Brief

journal homepage: www.elsevier.com/locate/dib

Data Article

The PaleoArchiNeo (PAN) human brain atlas: A dataset on a standard neuroanatomical MRI template following a phylogenetic approach

M. Zhernovaia[a], M. Dadar[b,c], S. Mahmoud[a], Y. Zeighami[b,c], J. Maranzano[a,b,*]

[a] Anatomy Department, Université du Québec à Trois-Rivières
[b] McConnel Brain Imaging Center, Montreal Neurological Institute, McGill University
[c] Department of Psychiatry, McGill University

ARTICLE INFO

Article history:
Received 3 March 2021
Revised 28 October 2021
Accepted 19 January 2022
Available online 23 January 2022

Keywords:
Atlas
Human brain
Cerebral cortex
MRI
Phylogenetic
Paleocortex
Archicortex
Neocortex

ABSTRACT

Cortical atlases provide consistent divisions of the human cortex into areas that have common structural as well as meaningful and distinctive functional characteristics. They constitute a fundamental tool to study and quantify changes in healthy and pathological states. Historically, the most widely used atlases follow the cytoarchitecture described by Brodmann and/or the myeloarchitectonic characteristics described by Vogt-Vogt. These histological approaches have since been combined to the standard anatomical nomenclature of gyri and sulci, referring to the corresponding cytoarchitectonic area(s) present in a gyrus, when applicable or necessary (e.g. area 4 of Brodmann in the pre-central gyrus). More recently, common functional features depicted by resting state functional MRI have guided the division of the cortex into functional regions of interest. However, to date, there are no human MRI atlases that divide the cortex considering the common evolutionary changes experienced by the mammalian cortex.

* Corresponding author at: University of Québec in Trois-Rivières, Department of Anatomy. Pavillon Léon-Provancher. Local 3507. 3351, boulevard des Forges, Trois-Rivières, Québec, Canada. G8Z 4M3. - McGill University, Department of Neurology and Neurosurgery, Montréal Neurological Institute. 3801 Rue University, Room WB327, Montréal, Québec, Canada, H3A 2B4.

E-mail addresses: josefina.maranzano@uqtr.ca, josefina.maranzano@mcgill.ca (J. Maranzano).
Social media: @Dadar (M. Dadar)

https://doi.org/10.1016/j.dib.2022.107863

Hence, the present dataset describes the PaleoArchiNeo (PAN) Human Brain, a voxel-based atlas that divides the human cortex into five regions of interest (ROIs) following a phylogenetic approach: 1- archicortex, 2- paleocortex, 3- peri-archicortex, 4- proisocortex, 5- neocortex, and thirty neocortical sub-ROIs that follow the gyral *Terminologia Anatomica*.The masks of the ROIs and sub-ROIs were segmented on the T1-weighted MNI ICBM 152 2009c symmetric average brain MRI model, the latest version of the most widely used standard brain template. The segmentations have been performed manually by anatomist experts, following the MRI anatomical landmarks that have been previously described, correlated, and validated with histology by other groups.

Specifications Table

Subject	Neuroanatomy
Specific subject area	Cortical human brain atlas
Type of data	Cortical masks of the regions of interest that constitute the PAN-Human Brain Atlas, manually segmented on the T1-weighted MNI ICBM 152 2009c symmetric average brain MRI model
How data were acquired	1.5T Magnetic resonance imaging
Data format	MINC2 and NIFTI
Parameters for data collection	The average template (MNI ICBM 152 2009c) as well as CerebrA labels were acquired from https://doi.gin.g-node.org/10.12751/g-node.be5e62/
Description of data collection	The data in this manuscript consists of: - The open-source International Consortium for Brain Mapping of the Montreal Neurological Institute (MNI-ICBM) 2009c average template - Manual masks created by the authors, marking the voxels of each cortical anatomical region of interest - Figs. 1 of the manuscript consists of a schematic representation of the subdivisions of the human cerebral cortex into paleocortex, archicortex, periarchicortex, proisocortex, and neocortex - Figs. 2 to 7 of the manuscript consist of snapshots of specific masks created by the authors superimposed on the MNI-ICBM template, to indicate some specific anatomical landmarks - Fig. 8 of the manuscript consists of multiple snapshots of all the masks created by the authors, to illustrate the full cortical segmentation
Data source location	McGill University, Montreal, Quebec, Canada. Université du Québec à Trois-Rivières, Trois-Rivières, Quebec, Canada.
Data accessibility	The average template (MNI ICBM 152 2009c) as well as CerebrA masks can be accessed at https://doi.gin.g-node.org/10.12751/g-node.be5e62/ All the masks of the PAN Human Brain Atlas can be accessed at https://doi.gin.g-node.org/10.12751/g-node.b4vh7k/

Value of the Data

- To date, there has been no MRI-based human brain atlas following a phylogenetic approach. Some groups have developed detailed segmentations of the hippocampus and amygdala. Others have described the segmentation of the piriform cortex. However, these different parcels have never been consistently grouped together considering their common evolutionary origin and were not based on a consistent and specific average template. Our atlas has combined anatomical and MRI cortical knowledge and translated it into a single atlas in a standard common space that considers phylogeny as the classification factor.

- This atlas will serve the neuroscientific research community interested in using MRI to quantify changes in the human brain, either in healthy populations or in pathological states. The atlas masks are voxel-based and constructed in a widely used average-open-source T1-weighted MRI template, which allows the registration of single individual MRI scans to the template to extract regional features to investigate both individual and population characteristics.
- This atlas will enable the study of changes in areas of cortex with common characteristics regarding their evolutionary development. Neuroscientists and neurologists interested in neurodegenerative diseases could explore whether pathological changes detectable by MRI (e.g. functional MRI, deformation and voxel-based morphometry, magnetization transfer values) preferentially affect areas of cortex with a given evolutionary chronology.

1. Data Description

The dataset that constitutes this atlas is a collection of voxel-based cortical regions of interests (ROIs) segmented in the International Consortium for Brain Mapping of the Montreal Neurological Institute (MNI-ICBM) 2009c average template [1], available in minc and nifti format in the following repository: https://gin.g-node.org/Maryna.Zhernovaia/MRI/ [2]. The cortical ROIs were segmented following a phylogenetic approach that divides the cerebral cortex into five main regions of interest (ROIs): 1-archicortex, 2-paleocortex, 3-peri-archicortex 4-proisocortex, 5-neocortex [3]. Additionally, we divided the neocortex into thirty sub-regions of interest (sub-ROIs) following an anatomical gyri division, which include various sensory modalities, as well as motor and association cortices: 5.1.temporopolar, 5.2.post-central, 5.3.pre-central, 5.4.pericalcarine, 5.5.superior temporal, 5.6.middle temporal, 5.7.precuneus, 5.8.insular, 5.9.inferior parietal, 5.10.caudal anterior cingulate, 5.11.posterior cingulate, 5.12.lingual, 5.13.caudal middle frontal, 5.14.cuneus, 5.15.fusiform, 5.16.inferior temporal, 5.17.isthmus cingulate, 5.18.lateral occipital, 5.19.lateral orbitofrontal, 5.20.medial orbitofrontal, 5.21.paracentral, 5.22.pars opercularis, 5.23.pars orbitalis, 5.24.pars triangularis, 5.25.rostral anterior cingulate, 5.26.rostral middle frontal,5.27. superior frontal, 5.28. superior parietal, 5.29. supramarginal, and 5.30. transverse temporal cortex [2]. Note: the specific label numbers of the minc and nifti ROI masks are detailed in Table 1 as well as in a readme file in the repository.

During mammalian evolution, the archi- and paleocortex, also grouped under the name of allocortex (allocortex=cortex with a number of layers different than six), precede the development of the larger neocortex. The archicortex is represented by the hippocampus, formed by the Cornus Ammonis areas, dentate gyrus and subiculum, presubiculum, parasubiculum, entorhinal cortex, retrosplenial cortex, and a cortical band in the cingulate gyrus [3]. The paleocortex, which shares common characteristics with the three-layered general cortex of reptiles [4], is composed of the piriform region, as well as part of the amygdala, the olfactory cortex, the olfactory bulb, retrobulbar (anterior olfactory nucleus), olfactory tubercle and septal region [3].

The much younger human neocortex, also called isocortex, is characterised by the six cellular layers depicted by classical Nissl stains. It comprises the sensory areas (primary somatosensory, auditory and visual areas, secondary and tertiary sensory areas), multimodal association areas, and motor areas: primary and non-primary [3].

Finally, the areas of cortices between archi- paleo- and neocortex show a gradual transformation of cytoarchitecture, which allow the classification of these transitional areas as periarchicortex, adjacent to the archicortex, and proisocortex, between the periarchicortex and neocortex [5], see Fig. 1.

2. Experimental Design, Materials and Methods

The atlas was done following previously described MRI protocols [6–15] that provide a detailed description of the MRI anatomical landmarks, correlated with histological studies, necessary to segment the parcels included within each of our ROIs.

Table 1
ROIs names and numbers of the final labels in MINC format.

LABEL NAME	Atlas ID Right Hemisphere labels	Atlas ID Left Hemisphere labels	Number of voxels: volume in mm^3
archicortex: ROI 1	1	55	3317
paleocortex: ROI 2	2	56	1134
periarchicortex: ROI 3	3	57	2238
proisocortex: ROI 4	4	58	596
temporopolar cortex: ROI 5.1	5	59	3752
post-central cortex: ROI 5.2	6	60	12156
pre-central cortex: ROI 5.3	7	61	12541
pericalcarine cortex: ROI 5.4	8	62	3015
superior temporal cortex: ROI 5.5	9	63	13572
middle temporal cortex: ROI 5.6	10	64	17509
precuneus cortex: ROI 5.7	11	65	12736
insular cortex: ROI 5.8	12	66	7611
inferior parietal cortex: ROI 5.9	13	67	16518
caudal anterior cingulate: ROI 5.10	14	68	1587
posterior cingulate: ROI 5.11	15	35	3016
lingual gyrus cortex: ROI 5.12	16	36	8381
caudal middle frontal: ROI 5.13	17	37	6597
cuneus: ROI 5.14	18	38	3780
fusiform: ROI 5.15	19	39	7576
inferior temporal: ROI 5.16	20	40	8944
isthmus cingulate: ROI 5.17	21	41	2133
lateral occipital: ROI 5.18	22	42	12746
lateral orbitofrontal: ROI 5.19	23	43	7153
medial orbitofrontal: ROI 5.20	24	44	4417
paracentral: ROI 5.21	25	45	4266
pars opercularis: ROI 5.22	26	46	4356
pars orbitalis: ROI 5.23	27	47	2184
pars triangularis: ROI 5.24	28	48	4440
rostral anterior cingulate: ROI 5.25	29	49	1650
rostral middle frontal: ROI 5.26	30	50	10998
superior frontal: ROI 5.27	31	51	30276
superior parietal: ROI 5.28	32	52	9468
Supramarginal: ROI 5.29	33	53	8535
transverse temporal: ROI 5.30	34	54	1289

We performed these segmentations manually on the MNI-ICBM 2009c average template, which is the most recent version of the MNI-ICBM152 brain average [1] and provides a higher level of anatomical details. The MNI-ICBM152 non-linear model has two main advantages: 1) it was created from a large number of subjects; hence it represents the average anatomy of the population and is unbiased, unlike single-subject models [14], and 2) the left-right symmetric version enables interpretation of asymmetries that might be found in an analysis.

The sub-ROIs of the neocortical parcels (other than the temporopolar region, which was done fully manually) were based on the manual correction of the CerebrA atlas [1], by removing voxels of partial volume with the subarachnoid space cerebrospinal fluid (CSF) and juxtacortical white matter. We chose CerebrA because it was also created on the MNI-ICBM152 2009c average template, providing the perfect complement to our manually created labels.

Both, fully manual segmentations and correction of the CerebrA masks were done using the interactive software package 'Display', part of the MINC Tool Kit (https://github.com/BIC-MNI) developed at the McConnell Brain Imaging Center of the Montreal Neurological Institute. This program allows simultaneous viewing and segmentation in the coronal, sagittal and axial planes. Each window allows zooming in and out and a painting tool allows marking voxels with a given color (label/mask number). All the labels created for the atlas consist of cortical gray matter only.

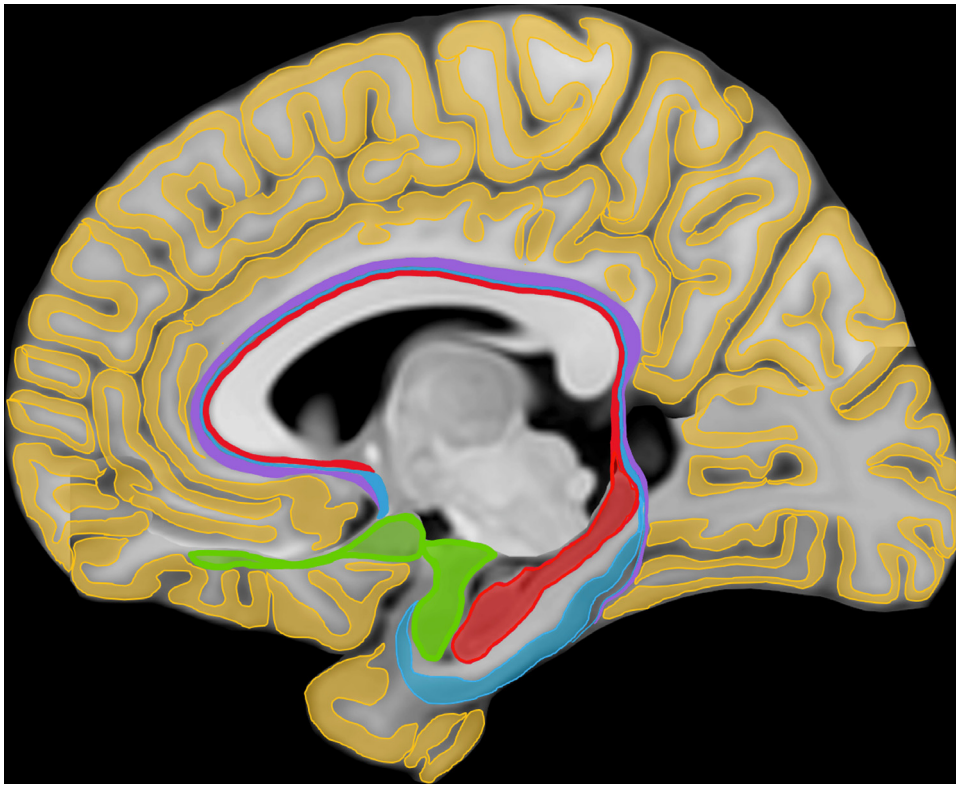

Fig. 1. Schematic representation of the subdivisions of the human cerebral cortex into paleocortex (in green), archicortex (in red), periarchicortex (in blue), proisocortex (in purple) and neocortex (in yellow). Inspired from Zilles and Amunts, 2012.
Note: we created a modified sagittal representation of the MRI template by fusing various parasagittal slices that allowed the delineation of the five ROIs in the same figure.

Note that this atlas, even if it follows a phylogenetic approach, has been created for use in images of the human brain exclusively and not in other species, since all MRI cortical regions are based on human anatomical landmarks correlated with human cytoarchitectonic characteristics of the specific cortices.

2.1. Anatomical MRI landmarks of each segmented ROI

ROI 1. Archicortex manual segmentation*:* we included the hippocampus, presubiculum, subiculum, parasubiculum, and entorhinal cortices. We did not attempt the segmentation of the pre- and supra-commissural (indusium griseum) hippocampal portions, because the resolution of the MRI brain template precluded its conclusive segmentation.

The hippocampus is traditionally divided into a posterior portion called the hippocampal tail (HT), a more anterior part called the hippocampal body (HB) and the most anterior, the hippocampal head (HH) [6].

The hippocampus included the dentate gyrus, the cornu ammonis (CA) regions, the part of the fasciolar gyrus that is adjacent to the CA regions. The white matter portions traditionally included in the MRI segmentation of the hippocampus [6] were excluded, because our atlas aims to exclusively include cortical gray matter. Hence, the fimbria, located at the superomedial

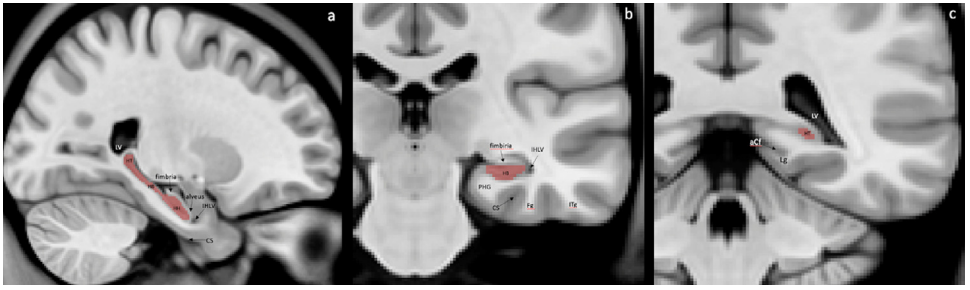

Fig. 2. MRI anatomical landmarks of the hippocampal limits. (a) Sagittal section with visualization of anterior, posterior, superior and inferior borders of the hippocampus; delineation of the fimbria that is excluded from the segmentation. (b) Coronal sections of the medial temporal lobe (MTL) with posterior end of the hippocampal body and (c) posterior end of the hippocampal tail.
IHLV= inferior horn of lateral ventriculus; LV= lateral ventriculus; CS= collateral sulcus; PHG= parahippocampal gyrus; Fg= fusiform gyrus; Itg= inferior temporal gyrus; aCf= anterior calcarine fissure; Lg= lingual gyrus; HB= hippocampal body; HT= hippocampal tail.

level of the HB and the alveus, which separates the HH from the amygdala at the supero-rostral level, were not included in our atlas.

The uncal recess of the inferior horn of the lateral ventricle (LV) and alveus served as landmarks for definition of the supero-anterior border of hippocampus [8]. The most posterior part of the HT was selected in the coronal plane, where an ovoid mass of gray matter (GM) is first visible inferio-medial to the trigone of the LV [6,14]. The lateral border of HB was identified by the inferior horn of the LV or the caudally adjacent WM: see Fig. 2.

The entorhinal cortex (EC) was segmented by selecting the coronal view and moving from anterior to posterior, from the posterior limit of the temporopolar cortex (described in section ROI.5.1.) towards the point of transition between the HH and HB (intralimbicus gyrus) [15]. The collateral sulcus (CS) was localised prior to the segmentation and served as a guide for the subsequent localisation of the first and last slices to be labelled [16]. If the CS was spreading rostral to the limen insulae (Li), then the anterior border of the EC was taken 2 mm posterior to the first appearance of the Li (grey matter); if the CS was shorter than the Li, then the anterior border was the rostral end of the CS [12,13]. The posterior limit was determined 1 mm posterior to the last slice containing the apex of the intralimbic gyrus [8,15]. The superio-medial limit of the EC was given by the sulcus semiannularis (ssa), and the lateral limit was always the midpoint of the medial bank of the CS: see Fig. 3.

ROI 2. Paleocortex manual segmentation:

The resolution of our MRI precluded the identification of the olfactory bulb and the distinction of the periamygdaloid cortex from the amygdaloid nuclei. Having a close relationship, both anatomically and functionally, the piriform cortex (PirC) and periamygdaloid cortex together with all the gray matter of the amygdala (AG) were considered in our atlas as a complex [7].

The most rostral portion was marked at the level of the Li (white matter-Li in the coronal view) [6,8].

Superomedially, the fundus of the sulcus semiannularis separates PirC from EC and superolateraly, the fundus of the entorhinal sulcus (es) separates the paleocortex from the substantia innominata. From the level of the Li posteriorly to the rostral end of the AG, the mediolateral extent of the piriform paleocortex occupies progressively more of the surface, (between 30% and 80% of that distance) [7], see Fig. 4.

Laterally, the gray matter of the AG transitions towards the ventral putamen. The posterior end was defined in the coronal plane at the level of the opening of the hippocampal fissure and at the point where grey matter appears superior to the alveus and laterally to the HH [6].

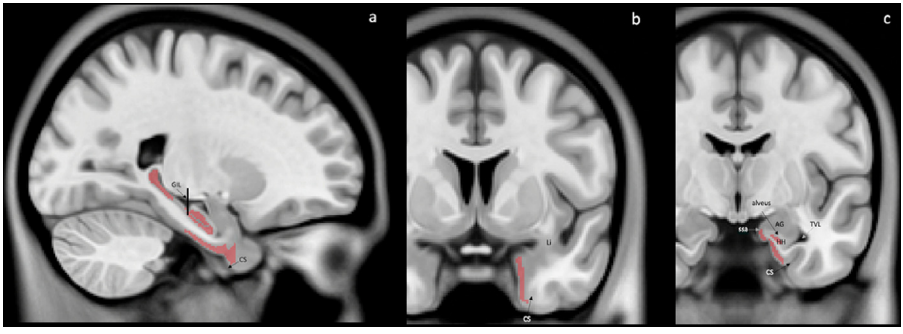

Fig. 3. MRI anatomical landmarks of the entorhinal cortex limits. (a) Sagittal section with visualization of anterior and posterior borders of EC. (b) Coronal view of the MTL at the level of the limen insulae and (c) at the level of uncal notch is visible. The perpendicular line indicates the apex of the gyrus intralimbicus.
Li= limen insulae GIL= gyrus intralimbicus; CS= collateral sulcus; AG= amygdala; ssa= sulcus semiannularis; TVL= temporal horn of lateral ventricle.

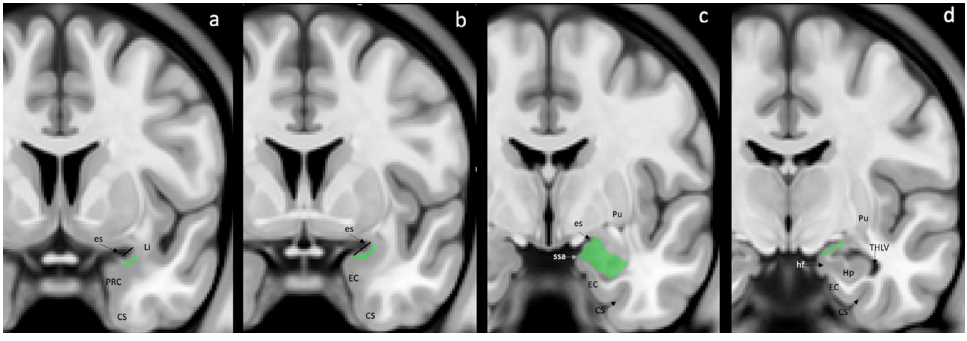

Fig. 4. MRI anatomical landmarks of the paleocortex limits. (a) Coronal section of the most rostral part of paleocortex at the level of limen insulae. At this level, piriform-cortical amygdala extends 30% of the distance between the entorhinal sulcus to the most convex point of the medial temporal cortex. (b) The piriform-cortical amygdala occupies 50% of the distance of the entorhinal sulcus – MTL convexity. (c) Coronal section at the level where the piriform-cortical amygdala extends from the entorhinal sulcus down to the sulcus semiannularis. (d) The most caudal section of paleocortex appearance at the level of hippocampal fissure opening.
es= entorhinal sulcus; Li= limen insulae; PRC= perirhinal cortex; CS= collateral sulcus; EC= entorhinal cortex; ssa= sulcus semiannularis; Pu= putamen; hf= hippocampal fissure; Hp= hippocampus; THLV= temporal horn of lateral. ventriculus.

ROI 3. Peri-archicortex manual segmentation:

We included the perirhinal and parahippocampal cortices [15]. The anterior segment of CS served for determining the rostral limit of the peri-archicortex (PeriAC) [16]. If the CS stretched further anterior than the Li, then the anterior tip of the CS was considered as the anterior border of the PeriAC [8]. If the CS was shorter or as long as the Li, then the border was determined to be 1 mm anterior to it. The most posterior part of parahippocampal cortex was defined as the first posterior slice where the pulvinar was no longer visible [8], and it was funnel-shaped, progressively merging with the retrosplenial region. The medial edge stretched from the shoulder of the medial bank of the CS to the medial apex of the parahippocampal gyrus. Laterally, the boundary between the perirhinal and inferotemporal cortices was at the lateral edge of the CS, but if two CS were present, then we considered the fundus of the more lateral CS [12,13], see Fig. 5.

ROI 4. Proisocortex manual segmentation:

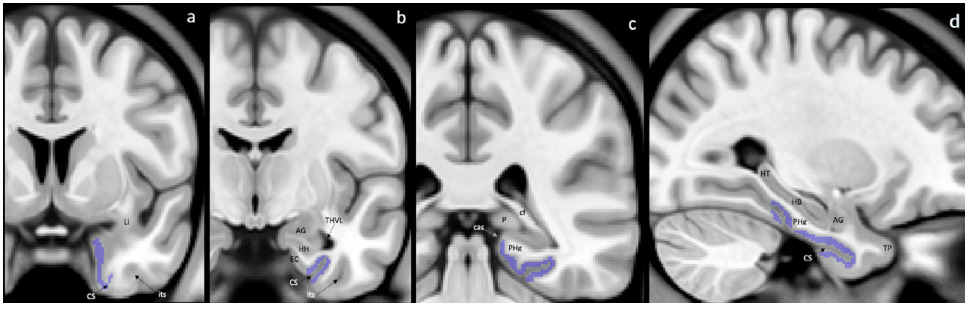

Fig. 5. MRI anatomical landmarks of the Peri-archicortex limits. (a) Coronal view of the temporal lobe section where the perirhinal cortex is segmented at the level of the collateral sulcus appearance. (b) Coronal section of the temporal lobe at the level of the perirhinal cortex boundaries with the entorhinal and inferior temporal cortices. (c) Coronal view of the posterior slide where the parahippocampal cortex presents. This is the most posterior level where the pulvinar is present. (d) Sagittal section with visualisation of the peri-archi cortex folded around the collateral sulcus.
Li= limen insulae; CS= collateral sulcus; its= inferior temporal sulcus; AG= amygdala; HH= hippocampal head; HB= hippocampal body; HT= hippocampal tail; EC= entorhinal cortex; THVL= temporal horn of ventriculus lateralis; cf= crus of the fornix; P= pulvinar; PHg= white matter portion of the parahippocampal gyrus; cas= calcarine sulcus; TP= temporal pole.

We included the gray matter of the supra- and sub-callosal areas of the anterior, middle and posterior cingulate gyrus (CinG) [10]. In the middle cingulate gyrus, we only considered the proisocortical section (IRd, area infraradiatadorsalis) [3] which is immediately adjacent to the location of the indusium griseum and perpendicular to the isocortical part of the cingulate gyrus that occupies the medial surface of the hemisphere (MR, area mediorata) [11].

The anterior limit was defined when the CinG was no longer present anterior to the corpus callosum. The gray matter of the CinG around the splenium of the corpus callosum formed the posterior border of proisocortex. Medially, in the more anterior region, the cortex was limited by gray matter of the superior shoulder of the callosal sulcus (CalS) (gray matter of the CinG), and in the more posterior region by the ventral shoulder of CalS (gray matter of the retrosplenial cortex) [3].

Laterally, the gray matter was segmented up to the deepest point of the bottom of the CalS (for the perigenou part) or at the level of the white matter of the CinG and deepest point of the calcarine fissure for the middle and posterior parts respectively: see Fig. 6.

ROI. 5.1. Temporopolar neocortex manual segmentation

The anterior limit was determined as the most prominent part of the temporal pole where the grey matter of the temporal cortex is first visible in the middle cranial fossa [8]. The visualization of the CS or gray matter of the Li defined the posterior border. The superolateral end was determined by the fundus of the temporo-polar sulcus (tps) and thus, the gyrus of Schwalbe [15] and the inferolateral limit was given by the medial bank of inferior temporal sulcus [12,13], see Fig. 7.

ROI 5.2. Post-central gyral cortex (somatosensory)

Corresponding to the somatosensory region, which was modified from the CerabrA atlas [1], by removing partial volume voxels adjacent to CSF and WM of the original masks labeled as 13 (right hemisphere) and 64 (left hemisphere) of the CerebrA atlas. The editing of the CerebrA mask was done using Display, which allowed saving our final atlas mask of the post central gyral cortex.

ROI 5.3. pre-central cortex (motor)

The original mask of the CerebrA atlas [1] was uploaded using Display and all the voxels of partial volume with either the adjacent juxtacortical white matter or the sulci cerebrospinal fluid were removed for regions 35 (right hemisphere) and 86 (left hemisphere) from CerebrA. The corrected mask was saved as the final atlas label for the pre-central gyrus.

ROI 5.4. pericalcarine cortex (visual)

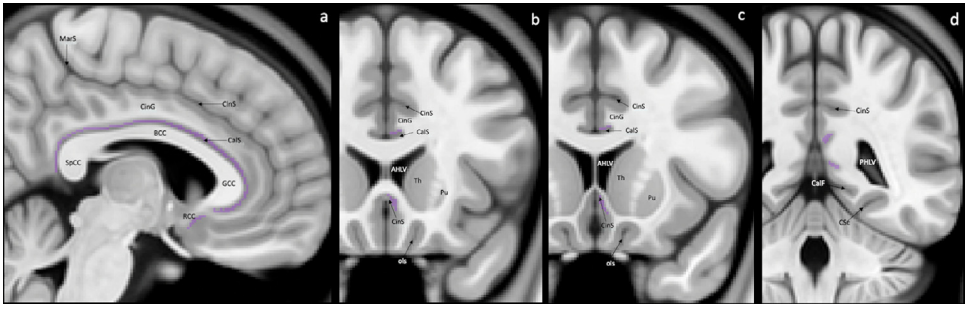

Fig. 6. MRI anatomical landmarks of the proisocortex limits. (a) Sagittal view of medial surface of a hemisphere, visualizing supra- and sub-callosal areas of anterior, middle and posterior cingulate gyrus where the proisocortex is present. (b) Coronal section of subcollosal CinC transition to subgenual CinC at the level where the putamen is first visualized within the basal ganglia. (c) Coronal view of the subgenual region at the level of the last slice after which the CinG is no longer present. (d) Coronal section of posterior CinC at the level of calcarine fissure.
GCC= genu corpus collosum; BCC= body corpus collosum, SpCC= splenium corpus collosum; RCC= rostrum corpus collosum; CalS= callosal sulcus; CinS= cingulate sulcus; CinG= cingulate gyrus; MarS= marginal sulcus; AHLV= anterior horn of lateral ventriculus; PHLV= posterior horn of lateral ventriculus; Th= thalamus; Pu= putamen; ols= olfactory sulcus; CalF= calcarine fissure; CSc= collateral sulcus caudal segment.

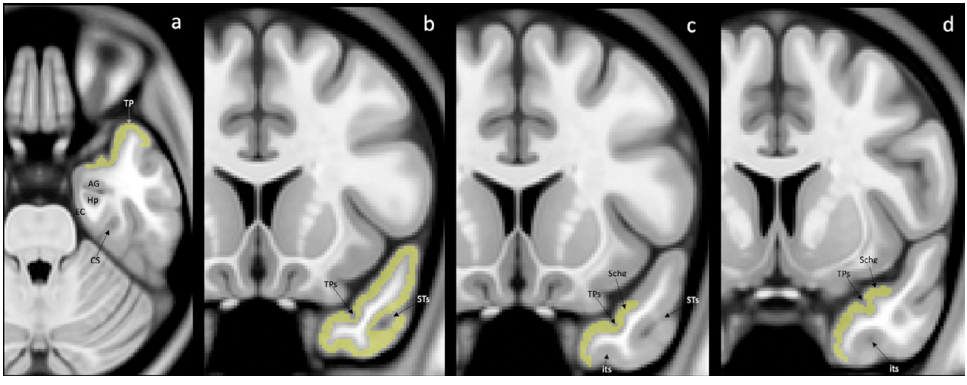

Fig. 7. MRI anatomical landmarks of the temporopolar neocortex limits. (a) Axial section of temporal lobe with visualisation of most prominent part of temporal pole. (b) The coronal view of anterior section of temporal lobe, when the inferior temporal sulcus was not yet visible and the section (c) where inferolateral and superolateral borders can be found. (d) The most posterior coronal section of temporopolar neocortex presence before limen insulae gray matter appearance. TP, temporal pole; AG, amygdala; Hp, hippocampus; EC, entorhinal cortex; CS, collateral sulcus; Schg, gyrus of Schwalbe; TPs, temporopolar sulcus; its, inferior temporal sulcus; STs, superior temporal sulcus.

A similar procedure as that described in point 5.3. was performed with the original masks labeled 6 (right hemisphere) and 57 (left hemisphere).

ROI 5.5. superior temporal cortex

A similar procedure as that described in point 5.3. was performed with the original masks 45 (right hemisphere) and 96 (left hemisphere). The area overlapping the segmentation of the temporopolar cortex was also excluded from the original CerebrA mask.

ROI 5.6. middle temporal cortex

A similar procedure as that described in point 5.3. was performed with the original masks 28 (right hemisphere) and 79 (left hemisphere). The area overlapping the segmentation of the temporopolar cortex was also excluded from the original CerebrA mask.

ROI 5.7. precuneus cortex (association)

A similar procedure as that described in point 5.3. was performed with the original masks 31 (right hemisphere) and 82 (left hemisphere).

ROI 5.8. insular cortex

A similar procedure as that described in point 5.3. was performed with the original masks 23 (right hemisphere) and 74 (left hemisphere).

ROI 5.9. inferior parietal cortex

A similar procedure as that described in point 5.3. was performed with the original masks 10 (right hemisphere) and 61 (left hemisphere).

ROI 5.10. caudal anterior cingulate cortex

A similar procedure as that described in point 5.3. was performed with the original masks 30 (right hemisphere) and 81 (left hemisphere).

ROI 5.11. posterior cingulate cortex

A similar procedure as that described in point 5.3. was performed with the original masks 47 (right hemisphere) and 98 (left hemisphere).

ROI 5.12. lingual cortex

A similar procedure as that described in point 5.3. was performed with the original masks 12 (right hemisphere) and 63 (left hemisphere).

ROI 5.13. caudal middle frontal cortex

A similar procedure as that described in point 5.3. was performed with the original masks 42 (right hemisphere) and 93 (left hemisphere).

ROI 5.14. cuneus cortex

A similar procedure as that described in point 5.3. was performed with the original masks 43 (right hemisphere) and 94 (left hemisphere).

ROI 5.15. fusiform cortex

A similar procedure as that described in point 5.3. was performed with the original masks 24 (right hemisphere) and 75 (left hemisphere).

ROI 5.16. inferior temporal cortex

A similar procedure as that described in point 5.3. was performed with the original masks 3 (right hemisphere) and 54 (left hemisphere).

ROI 5.17. isthmus cingulate cortex

A similar procedure as that described in point 5.3. was performed with the original masks 33 (right hemisphere) and 84 (left hemisphere).

ROI 5.18. lateral occipital cortex

A similar procedure as that described in point 5.3. was performed with the original masks 34 (right hemisphere) and 85 (left hemisphere).

ROI 5.19. lateral orbitofrontal cortex

A similar procedure as that described in point 5.3. was performed with the original masks 7 (right hemisphere) and 58 (left hemisphere).

ROI 5.20. medial orbitofrontal cortex

A similar procedure as that described in point 5.3. was performed with the original masks 15 (right hemisphere) and 66 (left hemisphere).

ROI 5.21. paracentral cortex

A similar procedure as that described in point 5.3. was performed with the original masks 16 (right hemisphere) and 67 (left hemisphere).

ROI 5.22. cortex of the pars opercularis

A similar procedure as that described in point 5.3. was performed with the original masks 32 (right hemisphere) and 83 (left hemisphere).

ROI 5.23. cortex of the pars orbitalis

A similar procedure as that described in point 5.3. was performed with the original masks 44 (right hemisphere) and 95 (left hemisphere).

ROI 5.24. cortex of the pars triangularis

A similar procedure as that described in point 5.3. was performed with the original masks 22 (right hemisphere) and 73 (left hemisphere).

ROI 5.25. rostral anterior cingulate cortex

A similar procedure as that described in point 5.3. was performed with the original masks 8 (right hemisphere) and 59 (left hemisphere).

ROI 5.26. rostral middle frontal cortex

A similar procedure as that described in point 5.3. was performed with the original masks 1 (right hemisphere) and 52 (left hemisphere).

ROI 5.27. superior frontal cortex

A similar procedure as that described in point 5.3. was performed with the original masks 38 (right hemisphere) and 89 (left hemisphere).

ROI 5.28. superior parietal cortex

A similar procedure as that described in point 5.3. was performed with the original masks 9 (right hemisphere) and 60 (left hemisphere).

ROI 5.29. supramarginal cortex

A similar procedure as that described in point 5.3. was performed with the original masks 51 (right hemisphere) and 102 (left hemisphere).

ROI 5.30. transverse temporal cortex (auditory)

A similar procedure as that described in point 5.3. was performed with the original masks 14 (right hemisphere) and 65 (left hemisphere).

Fig. 8 illustrates the different masks identifying the ROIs in a coronal section of the MNI-ICBM152 2009c T1-weighted average template.

The final masks of each ROI of the PaleoArchiNeo Human Brain Atlas are available at https://gin.g-node.org/Maryna.Zhernovaia/MRI/ [2]. Table 1 indicates the numbers of the MINC format masks of each ROI, in the right and left sides, and the number of voxels (volume in cubic milimeters) of each ROI.

The T1w template is available at http://nist.mni.mcgill.ca/?p=904 and https://gin.g-node.org/anamanera/CerebrA [1]. The imaging data is available in compressed MINC [17] and NIfTI formats.

Note that the masks of this atlas were intended to segment cortical GM voxels exclusively and avoid partial volume effects of neighboring CSF and WM voxels, resulting in relatively small masks for certain cortical areas, namely the proisocortex (masks 4 and 58). However, researchers using the PAN-atlas for applications that would require a more generous segmentation (e.g. for fMRI analyses) may choose to dilate the masks of specific ROIs (e.g. using dilation operators from itk_morph or mincmorph tools available at https://github.com/BIC-MNI/minc-toolkit-v2), as they deem necessary, according to their specific research question and experimental design. Further, manual correction of the masks after registration to specific single-subject scans is possible following the anatomical guidelines presented for the proisocortex area.

2.2. Validation

2.2.1. Intra-rater variability assessment

The manual segmentations of the archicortex, paleocortex, periarchicortex, proisocortex, and temporopolar cortex were performed by M.Z.

The correction of the CerebrA masks that were used as the starting point for the various neocortical areas considered in our atlas were performed by J.M.

All segmentations (either fully manual or the correction of pre-existing masks) were done twice, to allow the assessment of the intra-rater variability using Dice Kappa similarity index, which determines the proportion of voxels that are common (in the same spatial location) to the two masks. A Dice Kappa of 1 indicates a perfect spatial overlap, whereas a Dice Kappa of 0 implies no overlap between the two masks.

The Dice Kappa values of the different ROIs were as follows: 0.85 for the archicortex, 0.81 for the paleocortex, 0.69 for the periarchicortex, 0.64 for the proisocortex, 0.72 for the neocortical temporopolar cortex, 0.94 for the neocortical post-central gyrus, 0.79 for the neocortical pre-central gyrus, 0.83 for the neocortical pericalcarine region, 0.81 for the neocortical superior temporal gyrus, 0.99 for the neocortical middle temporal gyrus, 0.95 for the neocortical precuneus region, 0.87 for the insular cortex, and 0.80 for the neocortical inferior parietal gyrus, indicating excellent intra-rater agreement.

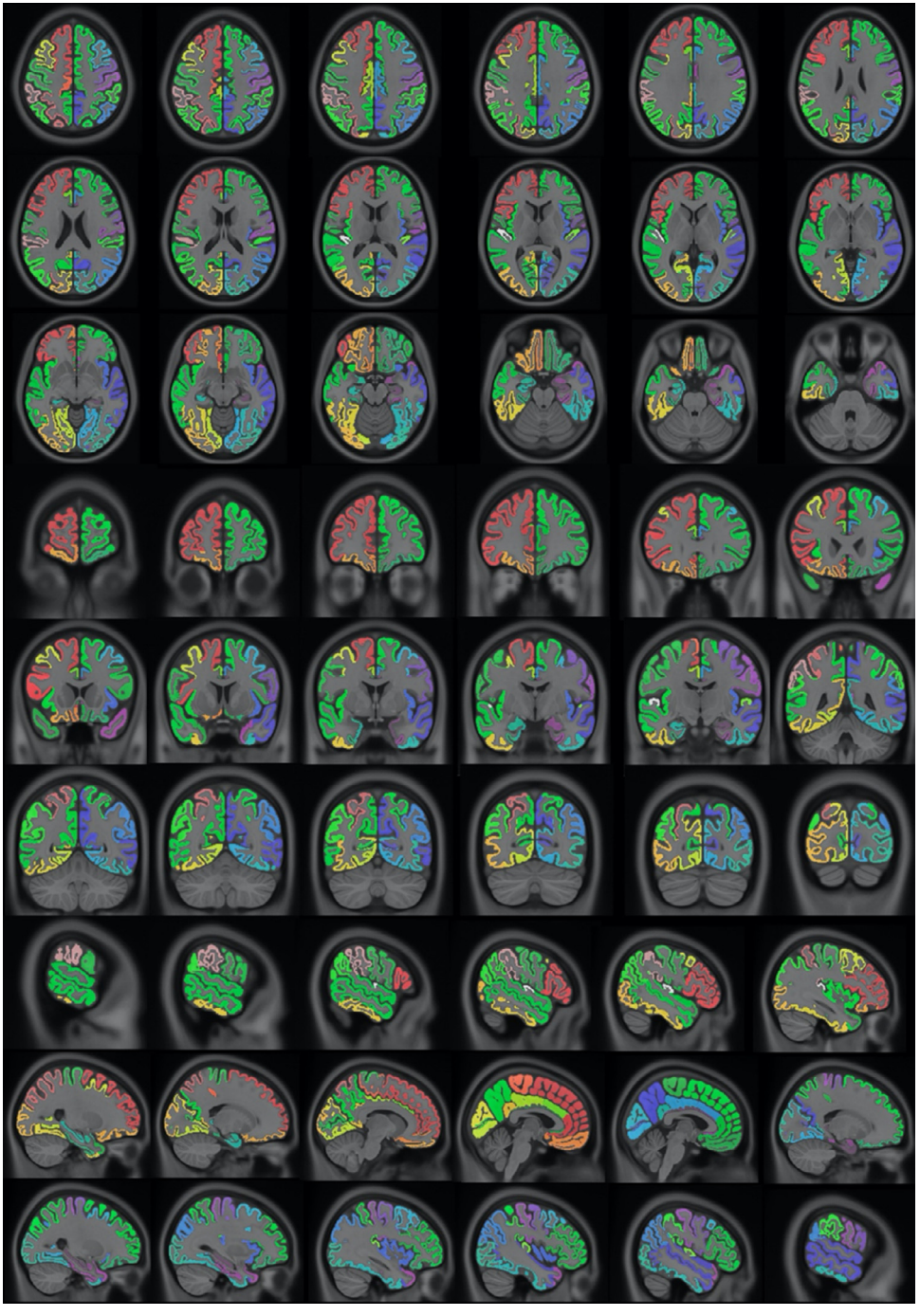

Fig. 8. From left to right, various inferior to superior axial slices (top three rows), right to left sagittal slices (bottom three rows), and anterior to posterior axial slices (three rows) of the masks of the ROIs.

The volumes of each cortical area, obtained in the first and second segmentation, showed a normal distribution, thus they were also assessed using a pair t-test and Pearson correlation coefficient. There was no statistically significant difference between the volumes obtained in the first and second segmentation (t=-0.6; p=0.6). The Pearson correlation coefficient was 0.99 ($p<0.0001$).

2.2.2. Inter-rater variability assessment

All the cortical areas were also independently segmented by a second rater to assess inter-rater variability also using the Dice Kappa similarity index.

The manual segmentations of the archicortex, paleocortex, periarchicortex, proisocortex, and temporopolar cortex were also segmented by J.M. an expert neuroanatomist with more than 15 years of experience in segmentation of the brain structures on MRI scans.

The corrections of the CerebrA neocortical masks were also performed by M.Z. a specialist in neuroanatomy who has two years of experience in cortical segmentation on MRI scans.

The Dice Kappa values of the different ROIs were as follows: 0.91 for the archicortex, 0.89 for the paleocortex, 0.82 for the periarchicortex, 0.81 for the proisocortex, 0.85 for the neocortical temporopolar cortex, 0.80 for the neocortical post-central gyrus, 0.79 for the neocortical pre-central gyrus, 0.86 for the neocortical pericalcarine region, 0.82 for the neocortical superior temporal gyrus, 0.79 for the neocortical middle temporal gyrus, 0.82 for the neocortical precuneus region, 0.84 for the insular cortex, and 0.80 for the neocortical inferior parietal gyrus, indicating excellent inter-rater agreement.

The volumes of each cortical area obtained by the two raters were also assessed using an independent t-test and Pearson correlation coefficient. There was no statistically significant difference between the volumes obtained by the two raters (t=-0.2; p=0.9). The Pearson correlation coefficient was 0.99 ($p<0.0001$).

Considering the inter-rater variability presented above, the set of masks created by either reader provides an equivalent set of masks of the atlas. The final masks available in the repository include the manual masks created by MZ, and the neocortical sub-ROIs' masks created by JM.

Ethics Statement

The present work did not involve the use of human subjects, nor animal experiments.

CRediT Author Statement

Maryna Zhernovaia: Study concept and design, manual segmentation of the labels, analysis and interpretation of the data, drafting and revision of the manuscript; **Mahsa Dadar**: Study concept and design, analysis and interpretation of the data, revising the manuscript; **Sawsan Mahmoud**: analysis and interpretation of the data, revising the manuscript; **Yashar Zeighami**: analysis and interpretation of the data, revising the manuscript; **Josefina Maranzano**: Study concept and design, manual correction of the labels and supervision of the manual segmentations, analysis and interpretation of the data, drafting and revision of the manuscript

Declaration of Competing Interest

The authors declare no competing interests.

References

[1] A. Manera, M. Dadar, V. Fonov, DL Collins, CerebrA: Accurate registration and manual label correction of the Mindboggle-101 atlas for the MNI-ICBM152 template, G-Node (2020), doi:10.12751/g-node.be5e62.

[2] M. Zhernovaia, M. Dadar, S. Mahmoud, Y. Zeighami, J. Maranzano, PhyloBrain atlas: a cortical brain MRI atlas following a phylogenetic approach, G-Node (2020), doi:10.12751/g-node.b4vh7k.

[3] JK. Mai, G. Paxinos, The human nervous system, Elsevier Academic Press, Amsterdam, 2012.

[4] E. Klingler, Development and organization of the evolutionarily conserved three-layered olfactory cortex, eNeuro 4 (1) (2017).

[5] K. Fleischhauer, Electroencephalogr. Clin. Neurophysiol. 41 (4) (1976) 448-448.

[6] JC. Pruessner, LM. Li, W. Serles, M. Pruessner, DL. Collins, N. Kabani, S. Lupien, AC. Evans, Volumetry of hippocampus and amygdala with high-resolution MRI and three-dimensional analysis software: minimizing the discrepancies between laboratories, Cereb. Cortex 10 (4) (2000) 433–442.

[7] PM. Gonçalves Pereira, R. Insausti, E. Artacho-Pérula, T. Salmenperä, R. Kälviäinen, A. Pitkänen, MR volumetric analysis of the piriform cortex and cortical amygdala in drug-refractory temporal lobe epilepsy, AJNR Am. J. Neuroradiol. 26 (2) (2005) 319–332.

[8] E. Frankó, AM. Insausti, E. Artacho-Pérula, R. Insausti, C. Chavoix, Identification of the human medial temporal lobe regions on magnetic resonance images, Hum. Brain Mapp. 35 (1) (2014) 248–256.

[9] S. Mikhael, C. Hoogendoorn, M. Valdes-Hernandez, C. Pernet, A critical analysis of neuroanatomical software protocols reveals clinically relevant differences in parcellation schemes, Neuroimage 170 (2018) 348–364.

[10] LM. McCormick, S. Ziebell, P. Nopoulos, M. Cassell, NC. Andreasen, M. Brumm, Anterior cingulate cortex: an MRI-based parcellation method, Neuroimage 32 (3) (2006) 1167–1175.

[11] N. Palomero-Gallagher, H. Mohlberg, K. Zilles, B. Vogt, Cytology and receptor architecture of human anterior cingulate cortex, J. Comp. Neurol. 508 (6) (2008) 906–926.

[12] JC. Pruessner, S. Köhler, J. Crane, M. Pruessner, C. Lord, A. Byrne, N. Kabani, DL. Collins, AC. Evans, Volumetry of temporopolar, perirhinal, entorhinal and parahippocampal cortex from high-resolution MR images: considering the variability of the collateral sulcus, Cereb. Cortex 12 (12) (2002) 1342–1353.

[13] R. Insausti, K. Juottonen, H. Soininen, AM. Insausti, K. Partanen, P. Vainio, MP. Laakso, A. Pitkänen, MR volumetric analysis of the human entorhinal, perirhinal, and temporopolar cortices, AJNR Am. J. Neuroradiol. 19 (4) (1998) 659–671.

[14] SL. Ding, JJ. Royall, SM. Sunkin, L. Ng, BA. Facer, P. Lesnar, A. Guillozet-Bongaarts, B. McMurray, A. Szafer, TA. Dolbeare, A. Stevens, L. Tirrell, T. Benner, S. Caldejon, RA. Dalley, N. Dee, C. Lau, J. Nyhus, M. Reding, ZL. Riley, D. Sandman, E. Shen, A. van der Kouwe, A. Varjabedian, M. Wright, L. Zöllei, C. Dang, JA. Knowles, C. Koch, JW. Phillips, N. Sestan, P. Wohnoutka, HR. Zielke, JG. Hohmann, AR. Jones, A. Bernard, MJ. Hawrylycz, P.R. Hof, B. Fischl, ES. Lein, Comprehensive cellular-resolution atlas of the adult human brain, J. Comp. Neurol. 524 (16) (2016) 3127–3481.

[15] S. Ulmer, O. Jansen, FMRI: basics and clinical applications, Springer, Berlin, 2013.

[16] SC. Huntgeburth, M. Petrides, Morphological patterns of the collateral sulcus in the human brain, Eur. J. Neurosci. 35 (8) (2012) 1295–1311.

[17] RD. Vincent, P. Neelin, N. Khalili-Mahani, AL. Janke, VS. Fonov, SM. Robbins, L. Baghdadi, J. Lerch, JG. Sled, R. Adalat, D. MacDonald, AP. Zijdenbos, DL. Collins, AC. Evans, MINC 2.0: a flexible format for multi-modal images, Front. Neuroinformat. 10 (35) (2016).